frontiers in Materials

ORIGINAL RESEARCH
published: 06 October 2021
doi: 10.3389/fmats.2021.717251

Structure and Magnetization of Strontium Hexaferrite ($SrFe_{12}O_{19}$) Films Prepared by Pulsed Laser Deposition

*M. Khojaste khoo and P. Kameli**

Department of Physics, Isfahan University of Technology, Isfahan, Iran

M-type strontium hexaferrite (SrM) thin films show excellent magnetic properties and uniaxial magnetic anisotropy. We systematically investigated the magnetism of SrM films prepared by pulsed-laser deposition on different substrates [Al_2O_3 ($1\bar{1}02$), $SrTiO_3$ (100), ZnO (0001), and $LiNbO_3$ (0001)] at vacuum (10^{-4} Pa) and a substrate temperature of 800°C. Prepared films were annealed in air at a temperature of 1,000°C for 2 hours. This investigation determined the effect of annealing and different substrates on the morphology, strain, and hysteresis loops of the films. The prepared films were characterized using x-ray diffractometry, Raman spectroscopy, scanning electron microscopy, and superconducting quantum interference device (SQUID) magnetometry. X-ray diffraction analyses confirmed c-oriented growth along the out-of-plane direction in most films. We found that annealing causes enhanced crystallization in films and a significant increase in coercivity. The highest coercivity of ~11 KOe was measured for the film deposited on the Al_2O_3 ($1\bar{1}02$) substrate.

Keywords: hexaferrite, thin film, annealing, coercivity, magnetization

OPEN ACCESS

Edited by:
Ahmad Gholizadeh, Damghan University, Iran

Reviewed by:
Vincent Harris, Northeastern University, United States
Manish Kumar, Pohang University of Science and Technology, South Korea

****Correspondence:***
P. Kameli
kameli@cc.iut.ac.ir

Specialty section:
This article was submitted to Thin Solid Films, a section of the journal Frontiers in Materials

Received: *30 May 2021*
Accepted: *17 August 2021*
Published: *06 October 2021*

Citation:
Khojaste khoo M and Kameli P (2021) Structure and Magnetization of Strontium Hexaferrite ($SrFe_{12}O_{19}$) Films Prepared by Pulsed Laser Deposition. Front. Mater. 8:717251. doi: 10.3389/fmats.2021.717251

INTRODUCTION

M-type hexagonal ferrites are promising materials for various applications, including microwave devices, magnetic field sensors, and data storage (Díaz-Castañón et al., 2001; Chen and Harris, 2012). They have favorable electrical properties (Tang et al., 2016), high chemical stability, low production cost (Zi et al., 2008), and unique magnetic properties such as high magnetization, high values of coercivity, and strong uniaxial magnetic anisotropy (Harris, 2012; Zhang et al., 2014). In hexaferrite thin films, the easy axis of magnetization is usually along the c-axis, and thin films with c-axis orientation find utility in specialized applications (Zhang et al., 2019). Thin films that can be used for microwave filters (Sun et al., 2016), phase shifters (Wu, 2012), and delay lines must be fabricated with in-plane orientation (IPCA). However, thin films used for circulators and isolators must possess an out-of-plane c-axis (OCA) orientation (Özgür et al., 2009; Meng et al., 2012). Strontium M-type hexagonal ferrite (SrM) belongs to the magnetoplumbite phase of ferrites (Pullar, 2012; Jotania, 2014). Researchers have classified hexagonal ferrites according to the location of their constituent subunit blocks. SrM has a hexagonal structure with a space group of *P63/mmc* and consists of four blocks (RSR*S*), where S = $Fe_6O_8^{2+}$ and R = $MFe_6O_{11}^{2-}$ (Kimura, 2012; Chen et al., 2016). The asterisk (*) indicates that the subunit is rotated 180° around the crystallographic c-axis. At absolute zero temperature, the total magnetization of the unit cell is related to the number of Fe^{3+} ions.

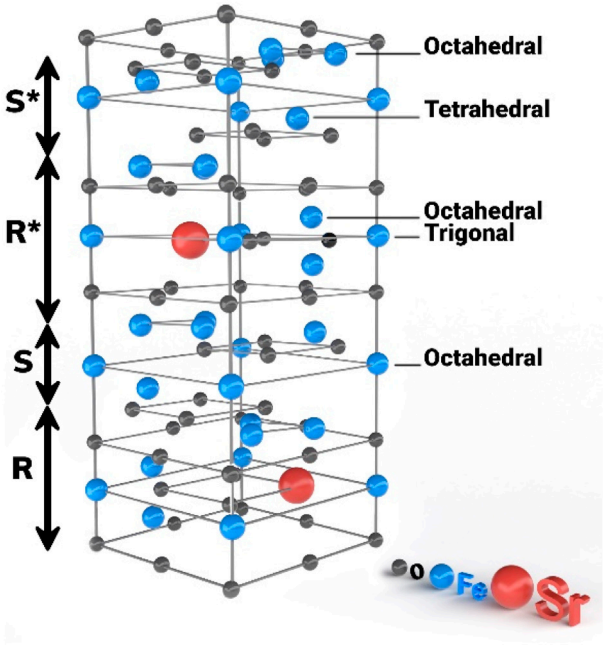

FIGURE 1 | Unit cell of SrM (contain S block and R block).

Fe^{3+} ions are divided equally between the two blocks. In the R block with a hexagonal structure, five ions are in an octahedral position (three spins up the magnetic moment and two spins down the magnetic moments), and one spin is up the magnetic moment on the bipyramidal site. The S block has a spinel structure with 4 of 6 Fe^{3+} ions in the octahedral position. The octahedral cations have spin-up moments with the two ions in the tetrahedral sites having spin-down moments (Kaur et al., 2006; Chen et al., 2017). There are eight spin-up and four spin-down moments in each unit cell, with the magnetic moment of each Fe^{3+} ion being 5 μ_B at absolute zero. Therefore, the magnetism of each unit cell is expected to be $4*5\mu_B = 20\mu_B$ (**Figure 1**) (Zi et al., 2008; Harris, 2012; Izadkhah et al., 2017).

Nowadays, investigators strive to determine deposition conditions that lead to improved performance. For example, deposition parameters that have been the foci of optimization studies include the choice of substrate (Hylton et al., 1993), substrate temperature (Xu et al., 2013a; Wei et al., 2020), working gas type and pressure (Masoudpanah et al., 2012), postdeposition annealing (Borisov et al., 2013), laser process conditions (Yu et al., 2020), and film thickness (Sun et al., 2016). Several common deposition techniques are available to obtain hexaferrite films of various crystallographic quality, including sol-gel (Masoudpanah and Seyyed Ebrahimi, 2012), molecular beam epitaxy (MBE) (Liu et al., 2010), liquid phase epitaxy (LPE) (Kranov et al., 2006; Wu et al., 2020), screen printing (Chen et al., 2006), radio frequency (RF) magnetron sputtering (Zhang et al., 2010; Xu et al., 2013a; Patel et al., 2018; Abuzir et al., 2020), direct current (DC) magnetron sputtering (Zhang et al., 2014; Zhang et al., 2019), spin-coating (Meng et al., 2014a; Meng et al., 2014b), and pulsed laser deposition (PLD) (Eason, 2007). The last method has been found to be a more effective technique than other reported methods for the deposition of oxide, nitride, and carbide thin films (Eason, 2007; Wei et al., 2016).

This work systematically investigated the effects of annealing on the structural and magnetic properties of SrM thin films deposited by PLD on various substrates. We discuss our results in terms of the effect of different magnetic anisotropy mechanisms on the structural and magnetic properties of SrM thin films.

EXPERIMENTAL

The films were deposited by PLD onto various single-crystal substrates from a sintered $SrFe_{12}O_{19}$ target prepared by the solid-state method. A KrF excimer laser producing monochromatic light at a wavelength of 248 nm at 25 ns pulses was used to produce a laser fluence of about 1.5 J/cm^2 at the surface of the ceramic target. A pulse repetition rate of 10 Hz was employed. The base pressure in the PLD chamber was 2×10^{-4} Pa, and the substrate temperature was 800°C. After deposition, the films were annealed at 1,000°C in air for 2 hours to further complete the film's crystallinity.

It is expected that the crystal structure and orientation of the substrate play an important role in determining the texture and properties of the films. Therefore, here we deposited SrM thin films on different substrates: Al_2O_3 ($1\bar{1}02$), STO (100), $LiNbO_3$ (0001), and ZnO (0001), which are assigned the following abbreviations in this article: SAlO, SSTO, SLNO, and SZnO, and the films annealed at 1,000°C are designated as AAlO, ASTO, ALNO, and AZnO. The thickness of all films was ~50 nm. The objective of the study was to determine optimum process parameters that would yield films of the highest crystal quality, magnetization, and magnetic anisotropy. θ–2θ X-ray diffraction (XRD) was carried out to evaluate thin film crystallinity, orientation, and strain. Moreover, Raman spectroscopy was also employed to investigate the strain in the thin films. The surface morphology of the films was examined using scanning electron microscopy (SEM). Most magnetic measurements were made using a 5 T SQUID magnetometer (MPMS 5 XL, Quantum Design) on films mounted in clear plastic straws with the magnetic field applied parallel or perpendicular to the film plane.

RESULTS AND DISCUSSIONS

Figure 2 shows the XRD patterns of films deposited on different substrates before and after heat treatment. This allows for the evaluation of the impact of the annealing treatment on the structural properties of SrM thin films, which indicates annealing can be used to improve crystallinity that may result in improved superior magnetic properties (Zheng et al., 2016). Also, the effect of different substrates is observed. The X-ray patterns and the known JCPDS card (01-080-1197) were compared, and the presence and identification of all

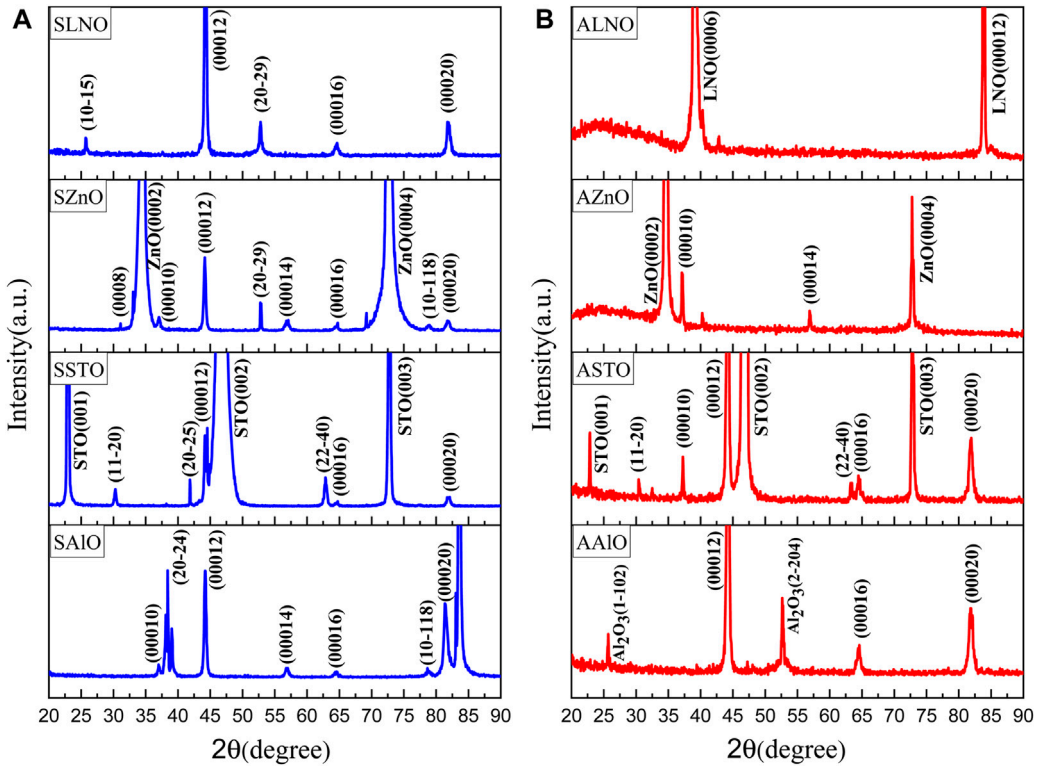

FIGURE 2 | (A) XRD patterns of films on different substrates **(B)** after annealing.

diffraction peaks confirmed the hexagonal structure (Chen et al., 2010). The X-ray diffraction pattern of the sample SAlO showed two different peaks being indexed to the ($h0\bar{h}l$) and (000l) planes of SrM, but after annealing AAlO film 000l peaks remained , and this film exhibited good crystallinity and good out-of-plane orientation of the c-axis. The film deposited on STO (100) indicated both in-plane ($hh2h0$) and out-of-plane (000l) orientations. The structure of the substrate plays a vital role in the formation of the film and its properties. STO substrate has a cubic structure, so the difference between the film's structure and the substrate and the mismatch of their lattice parameter increase the strain in the thin film and cause a scattered orientation. **Figure 2B** shows the XRD patterns of ASTO. As can be observed, the intensity of (000l) peaks increased, and a new peak, 00010, appeared, indicating improvement of out-of-plane orientation after annealing. The XRD pattern of AZnO represents a highly oriented (000l) direction due to the same hexagonal crystal structure of SrM and ZnO.

The XRD patterns of SLNO and ALNO show diffraction peaks that support the existence of out-of-plane crystal texture. Still, in the pattern of the annealed film, the intensity of SrM diffraction features diminish, indicating that most SrM has evaporated during annealing and only a small volume of the ferrite remains on the substrate. We discuss this point in the following sections.

In-plane lattice parameter a and out-of-plane lattice parameter c of the SrM film were calculated using the formula:

$$\frac{1}{d_{hkl}^2} = \frac{4}{3}\frac{\left(h^2 + hk + k^2\right)}{a^2} + \frac{l^2}{c^2}, \tag{1}$$

where d is the interplanar distance and h, k, and l are Miller indices. The bulk (target) lattice parameters are a = 5.914 and c = 23.283. We calculated the stain ratio for each film. The results are shown in **Table 1**. The in-plane and out-of-plane lattice parameters of the films on ALO, STO, and LNO substrates are less than the bulk value, indicating compressive strain. On the other hand, the films on the ZNO substrate are under tensile strain (Malek et al., 2015). As can be seen from **Table 1**, the strain increased after annealing.

In our work, we used Raman spectra to investigate the effect of strain on thin films after annealing (Wang et al., 2004) (**Figure 3**). In Raman spectroscopy, the incident phonons either gain quanta or lose quanta by interacting with the vibrational modes of the material. If it gains energy, it gets blue-shifted, and if it loses, it is red-shifted. The amount of the shift determines the energy of the phonon in the material. Raman spectroscopy is a powerful tool for ascertaining lattice strain (Lisfi and Williams, 2003). If the material lattice experiences compressive strain, the Raman shift increases; if it is under tensile strain, the Raman shift decreases. These shifts are called blue shift and red shift, respectively. Since the lattice constants of $SrFe_{12}O_{19}$ are larger than the AlO substrate, the strain created in the film should be compressive. The Raman spectra of the thin films (shown in **Figure 3A**) deposited on Al_2O_3 show a substantial peak at 672 cm^{-1}

TABLE 1 | Lattice parameters and strain ratio of the SrM films grown on different substrates.

Sample	In-plane parameter (a)	Strain ratio (a)%	Out-of-plane parameter (c)	Strain (c)%
SALO	5.890	−0.40	23.081	−0.87
AALO	5.832	−1.39	23.056	−-0.98
SSTO	5.907	−0.13	23.088	−0.84
ASTO	5.871	−0.74	23.097	−0.80
SLNO	5.837	−1.31	23.053	−0.99
SZnO	5.920	+0.10	23.497	+0.92
AZnO	5.929	+0.25	23.506	+0.96

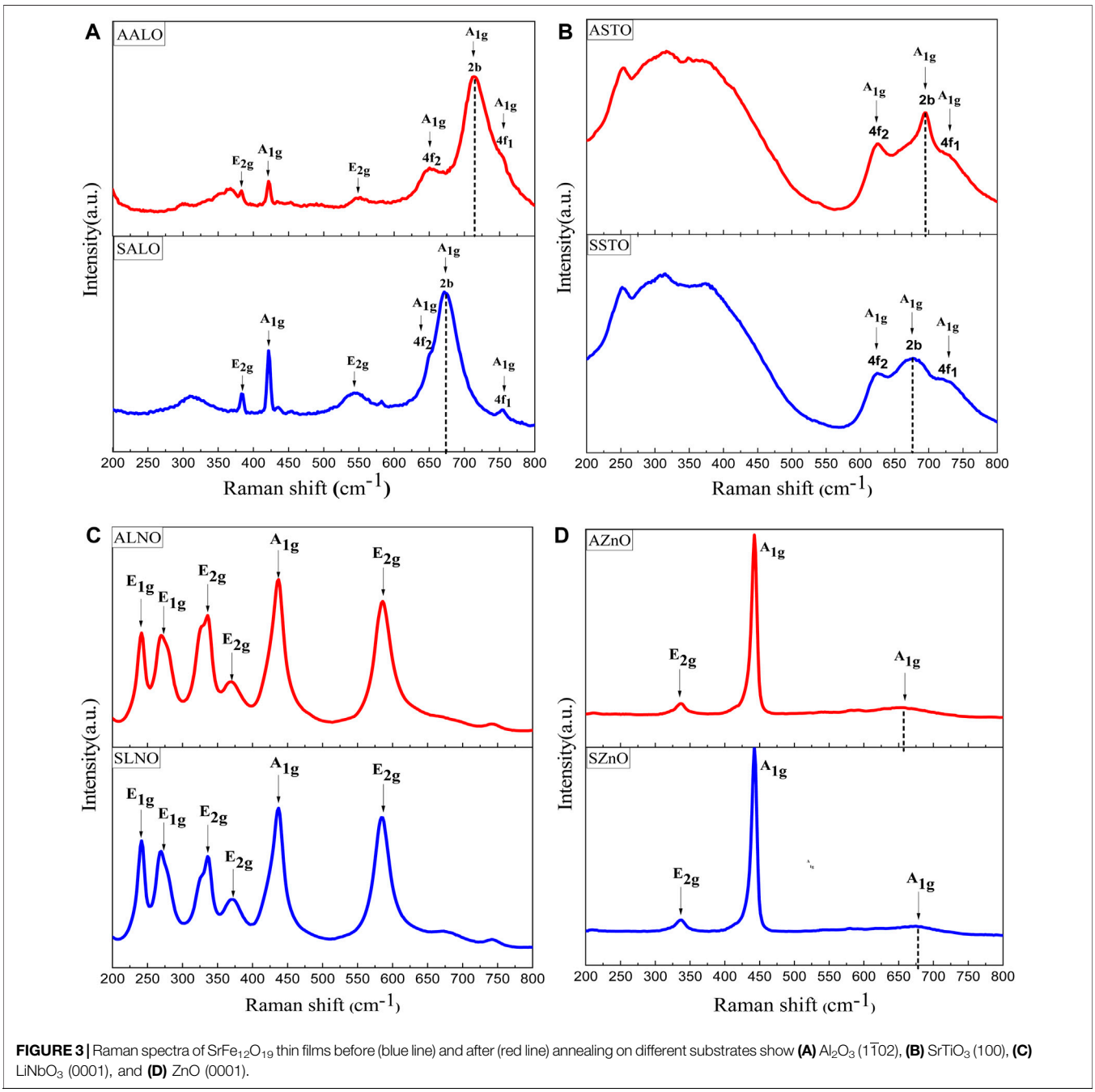

FIGURE 3 | Raman spectra of $SrFe_{12}O_{19}$ thin films before (blue line) and after (red line) annealing on different substrates show **(A)** Al_2O_3 ($1\bar{1}02$), **(B)** $SrTiO_3$ (100), **(C)** $LiNbO_3$ (0001), and **(D)** ZnO (0001).

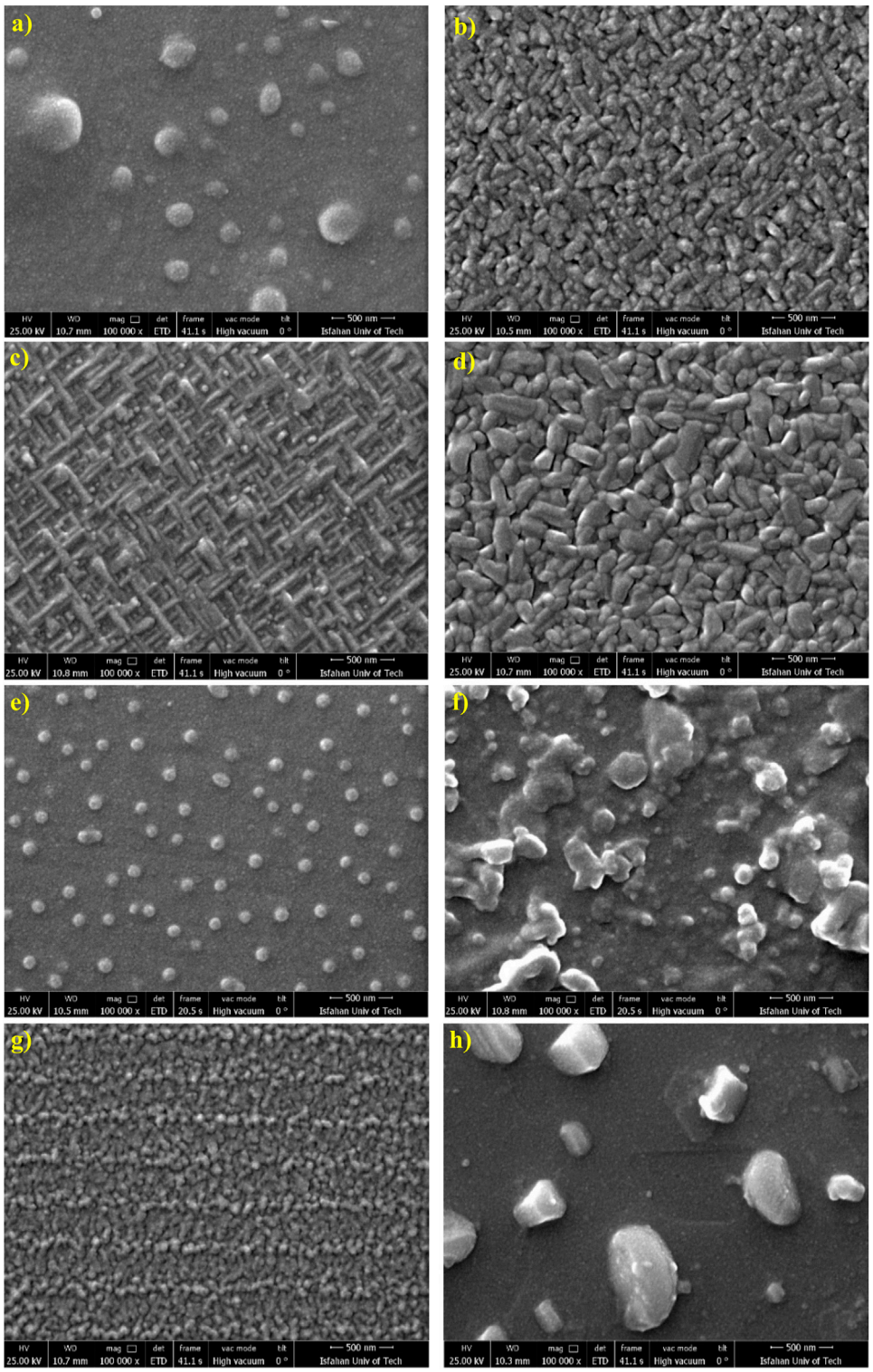

FIGURE 4 | SEM images of films. **(A)** Surface of film SALO, **(B)** surface of film AALO, **(C)** surface of film SSTO, **(D)** surface of film ASTO, **(E)** surface of film SZnO, **(F)** surface of film AZnO, **(G)** surface of film SLNO, and **(H)** surface of film ALNO.

(SAlO) related to the A_{1g} mode of SrM cm^{-1}SAlOwhich shifts to 715 cm^{-1} after annealing (AAlO), confirming the existence of a pronounced compressive strain (Kreisel et al., 1998; Zhang et al., 2017). Also, a blue shift is observed for films on STO substrates that increases with the annealing of the sample, but the shift is less than that for the film on the Al_2O_3 substrate. It can be observed in

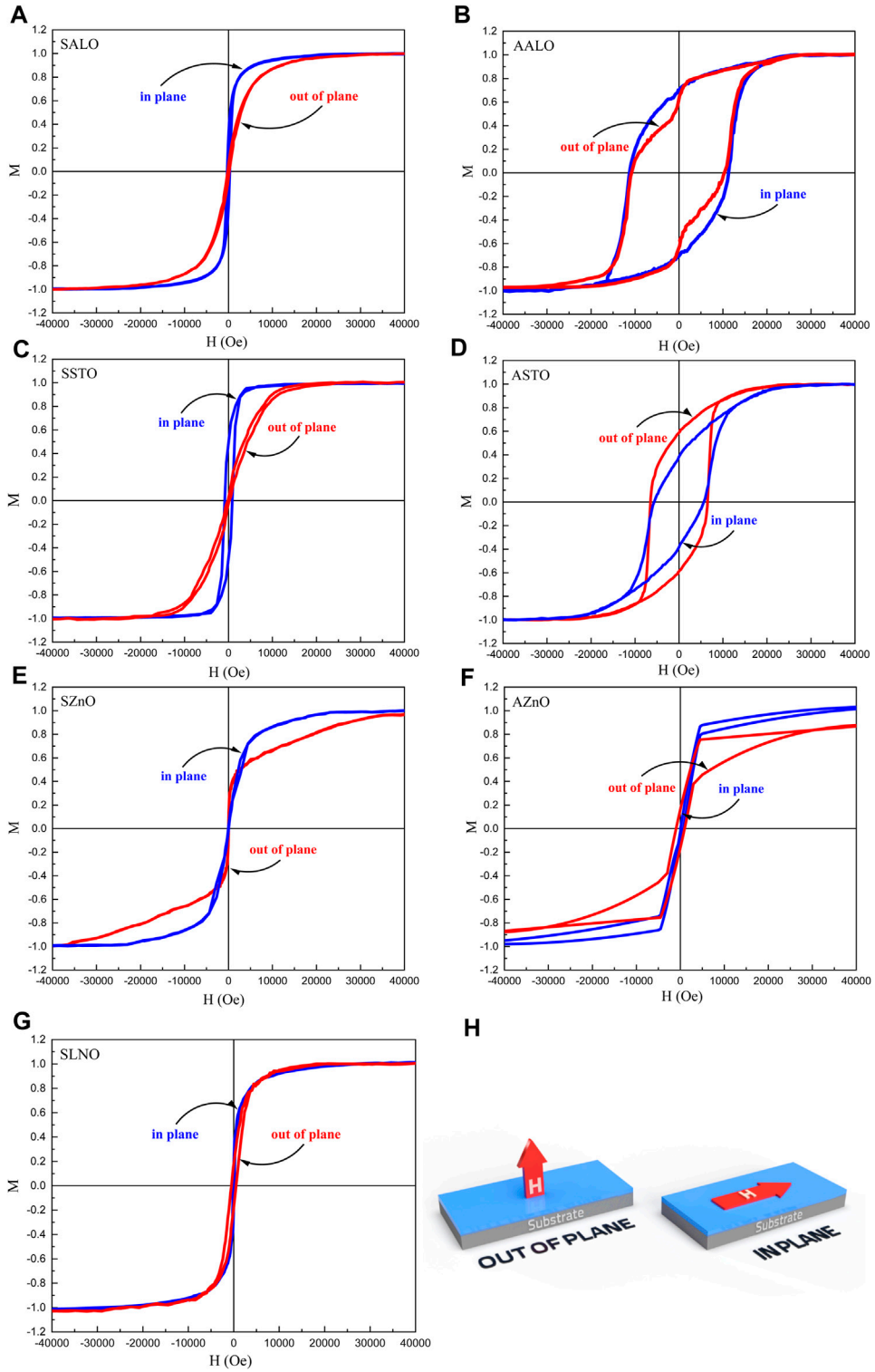

FIGURE 5 | Normalized magnetic hysteresis loops of films with various substrates, before annealing: **(A)** SALO, **(C)** SSTO, **(E)** SZnO, and **(G)** SLNO, and after annealing: **(B)** AALO, **(D)** ASTO, and **(F)** AZnO. **(H)** Schematic of the applied magnetic field direction during the M–H measurements of the SrM film.

Figure 3B that the peak (695 cm^{-1}) associated with the trigonal site of the SrM is relatively sharp, which shows that strontium ferrite films have an improved crystalline structure after annealing. In contrast, the Raman spectra shown in **Figure 3C** illustrate a red shift because the lattice parameter of ZnO is larger than SrM, and therefore, a tensile strain exists in these films,

TABLE 2 | Magnetic characteristics of the SrM films grown on different substrates in an applied magnetic field, parallel to (in-plane) or perpendicular to (out-of-plane) the c-axis of SrM.

Thin films	In-plane				Out-of-plane			
	H_c (O_e)	M_s (emu/cm^3)	M_r (emu/cm^3)	M_r/M_s	H_c (O_e)	M_s (emu/cm^3)	M_r (emu/cm^3)	M_r/M_s
SALO	298	227	66	0.29	182	237	13	0.05
AALO	11,252	146	102	0.70	10,557	141	88	0.62
SSTO	860	218	105	0.48	204	213	6	0.03
ASTO	5,642	250	96	0.38	6,495	238	140	0.59
SLNO	124	18	3	0.17	500	16	2.8	0.175
SZnO	58	152	2	0.01	25	108	8	0.07
AZnO	340	12	0	0	990	3	0.5	0.17

which increases with annealing. **Figure 3D** shows that for the films on LNO, the Raman peaks do not change markedly after annealing.

Figure 4 shows SEM micrographs of the surface morphology of as-deposited thin films and the films annealed at 1,000°C. It is known that ferrite microstructure depends on various parameters such as annealing temperature and time, substrate type, and deposition temperature. The SEM images illustrate an increase in the average grain sizes upon annealing. It has been shown by others that strontium ferrite grains often appear acicular-like or platelet-like (Xu et al., 2013b). According to the literature, we can determine the orientation of the c-axis from the shape and alignment of grains in SEM images. Platelet-like grains tend to have an out-of-plane orientation of the c-axis, while acicular-like grains have either an in-plane or a random orientation of the c-axis (Meng et al., 2014b). Therefore, nearly all the samples studied here have an out-of-plane orientation except for two samples SSTO and ASTO, whose grains are distributed randomly without a pronounced crystalline texture. As previously mentioned, among the films deposited on LNO, including those that were annealed, the SrM mostly evaporates, with few large grains visible on the substrate surface.

The magnetic properties of the strontium ferrite thin films were measured by a superconducting quantum interference device (SQUID) magnetometer. Magnetic hysteresis loops were measured with magnetic fields applied along the perpendicular and the in-plane directions to the films at room temperature (**Figure 5H**). The normalized hysteresis curves are shown in **Figure 5**. The magnetic parameters such as saturation magnetization (M_s), remanent magnetization (M_r), and coercivity (H_c) were determined from the M-H loops and are tabulated in **Table 2**. It was found that AAlO exhibits the maximum H_c (~11 KOe) compared to other film samples. **Figure 5** shows that annealing generally leads to increased H_c. We attribute this H_c enhancement to an increase in strain and crystallization in SrM thin films as confirmed by Raman spectroscopy (**Figure 3**) and SEM micrographs (see **Figure 4**). The SAlO film exhibits an in-plane easy axis (**Figure 5A**), but the c-axis of this sample is along the out-of-plane direction. The anisotropy in films was determined by competing anisotropy mechanisms, for instance, magnetocrystalline anisotropy, shape anisotropy, and magnetostriction (i.e., magnetic response to strain). In AlO, the in-plane anisotropy induced by the sample shape (i.e., surface dipoles) and strain, and the out-of-plane anisotropy induced by magnetocrystalline anisotropy are comparable. It seems the shape anisotropy energy begins to dominate, and this sample shows an in-plane easy direction. The shape anisotropy changes the magnetization direction to where the magnetostatic energy is minimal; thus, thin films have an in-plane shape anisotropy. In this sample, there is a lattice mismatch between the $SrFe_{12}O_{19}$ film and the substrate. The film lattice parameter is larger than the substrate. As a result, compressive strain appears in this sample results. It seems AAlO is more isotropic than other films, and the hysteresis loop of this film displays a characteristic reduced amplitude at low field. The out-of-plane hysteresis loop of AAlO presents an apparent two-step behavior, with the magnetization decreasing at a small return field. This anomaly in the magnetic hysteresis loop can be described by the participation of a surface anisotropy, different from the bulk because of the broken symmetry at the film surface (Lavorato and Winkler, 2016). This also can indicate a 2-phase material that could have resulted from the diffusion of Fe into the AlO and the formation of interface soft spinel (Chen et al., 2010). On the other hand, this change in slope signals the switching of a soft magnetic phase that is decoupled from the harder SrM phase.

The SSTO film indicates an in-plane anisotropy (**Figure 5C**), but the anisotropy changes after annealing and ASTO shows an out-of-plane anisotropy (**Figure 5D**). Alternatively, SZnO and AZnO illustrate very little coercivity (H_c). After annealing, the magnetic hysteresis loop of the sample AZnO shows little coercivity, and the remanence is nearly zero. The hysteretic magnetization is followed by the opening of the loop at high fields possibly due to the influence of uniaxial anisotropy (Gao et al., 2009) (**Figure 5E**).

The SLNO film does not show magnetic anisotropy. Since the LNO substrate is paramagnetic and a small amount of strontium ferrite material remains on the substrate surface after annealing, no magnetic hysteresis loops were observed for ALNO.

CONCLUSION

M-type strontium hexaferrite (SrM) thin films prepared by pulsed laser deposition on Al_2O_3 ($1\bar{1}02$), $SrTiO_3$ (100), ZnO

(0001), and $LiNbO_3$ (0001)) substrates were annealed in air at a temperature of 1,000°C and characterized by Raman spectroscopy, X-ray diffractometry, scanning electron microscopy, and SQUID magnetometry. These investigations indicated that annealing and different substrates have a critical effect on the morphology, strain, and hysteresis loops of the films. X-ray diffraction analyses confirmed the c-axis–oriented growth along the out-of-plane direction. We found that annealing causes enhanced crystallization of films and a significant increase in coercivity. The highest coercivity of ~11 KOe was measured for the film on Al_2O_3 ($1\bar{1}02$) substrate.

DATA AVAILABILITY STATEMENT

The original contributions presented in the study are included in the article/Supplementary Material. Further inquiries can be directed to the corresponding author.

AUTHOR CONTRIBUTIONS

MK fabricated the samples and carried out the experiment. MK wrote the draft of the manuscript. PK conceived the original idea, supervised the project, and revised the manuscript.

REFERENCES

Abuzir, A. R., Salman, S. A., and Mazher, J. (2020). Magnetron Sputtered Perpendicular Barium Hexaferrite Thin Films Produced by the Multilayered Method. *J. Supercond. Nov. Magn.* 33 (12), 3819–3825. doi:10.1007/s10948-020-05647-3

Borisov, P., Alaria, J., Yang, T., McMitchell, S. R. C., and Rosseinsky, M. J. (2013). Growth of M-type Hexaferrite Thin Films with Conical Magnetic Structure. *Appl. Phys. Lett.* 102, 032902. doi:10.1063/1.4776223

Chen, Z., and Harris, V. G. (2012). Ferrite Film Growth on Semiconductor Substrates towards Microwave and Millimeter Wave Integrated Circuits. *J. Appl. Phys.* 112 (8), 081101. doi:10.1063/1.4739219

Chen, Y., Geiler, A. L., Sakai, T., Yoon, S. D., Vittoria, C., and Harris, V. G. (2006). Microwave and Magnetic Properties of Self-Biased Barium Hexaferrite Screen Printed Thick Films. *J. Appl. Phys.* 99 (8), 08M904–4. doi:10.1063/1.2163288

Chen, Z., Yang, A., Mahalingam, K., Averett, K. L., Gao, J., Brown, G. J., et al. (2010). Structure, Magnetic, and Microwave Properties of Thick Ba-Hexaferrite Films Epitaxially Grown on GaN/Al2O3 Substrates. *Appl. Phys. Lett.* 96 (24), 242502–242504. doi:10.1063/1.3446867

Chen, D.-M., Li, Y.-X., Han, L.-K., Long, C., and Zhang, H.-W. (2016). Perpendicularly Oriented Barium Ferrite Thin Films with Low Microwave Loss, Prepared by Pulsed Laser Deposition. *Chin. Phys. B* 25, 068403–068406. doi:10.1088/1674-1056/25/6/068403

Chen, D., Chen, Z., Wang, G., Chen, Y., Li, Y., and Liu, Y. (2017). Effect of Al on the Microstructure, Magnetic and Millimeter-Wave Properties of High Oriented Barium Hexaferrite Thin Films. *J. Magnetism Magn. Mater.* 444, 7–11. doi:10.1016/j.jmmm.2017.07.090

Díaz-Castañón, S., Leccabue, F., Watts, B. E., Yapp, R., Asenjo, A., and Vázquez, M. (2001). Oriented PbFe12O19 Thin Films Prepared by Pulsed Laser Deposition on Sapphire Substrate. *Mater. Lett.* 47 (6), 356–361. doi:10.1016/S0167-577X(00)00266-4

Eason, R. (2007). *Pulsed Laser Deposition of Thin Films: Applications-Led Growth of Functional Materials*. Southampton, United Kingdom: John Wiley & Sons.

Gao, Q., Hong, G., Ni, J., Wang, W., Tang, J., and He, J. (2009). Uniaxial Anisotropy and Novel Magnetic Behaviors of CoFe2O4 Nanoparticles Prepared in a Magnetic Field. *J. Appl. Phys.* 105 (7), 07A516. doi:10.1063/1.3072019

Harris, V. G. (2012). Modern Microwave Ferrites. *IEEE Trans. Magn.* 48 (3), 1075–1104. doi:10.1109/TMAG.2011.2180732

Hylton, T. L., Parker, M. A., Coffey, K. R., and Howard, J. K. (1993). Properties of Epitaxial Ba-hexaferrite Thin Films on A-, R-, and C-plane Oriented Sapphire Substrates. *J. Appl. Phys.* 73, 6257–6259. doi:10.1063/1.354065

Izadkhah, H., Zare, S., Somu, S., Lombardi, F., and Vittoria, C. (2017). Utilizing Alternate Target Deposition to Increase the Magnetoelectric Effect at Room Temperature in a Single Phase M-type Hexaferrite. *MRS Commun.* 7 (2), 97–101. doi:10.1557/mrc.2017.36

Jotania, R. (2012). Crystal Structure, Magnetic Properties and Advances in Hexaferrites: A Brief Review. *AIP Conf. Proc.* 1621, 596–599. doi:10.1063/1.4898528

Kaur, B., Bhat, M., Licci, F., Kumar, R., Kulkarni, S. D., Joy, P. A., et al. (2006). Modifications in Magnetic Anisotropy of M-type Strontium Hexaferrite Crystals by swift Heavy Ion Irradiation. *J. Magn. Magn. Mater.* 305 (2), 392–402. doi:10.1016/j.jmmm.2006.01.110

Kimura, T. (2012). Magnetoelectric Hexaferrites. *Annu. Rev. Condens. Matter Phys.* 3 (1), 93–110. doi:10.1146/annurev-conmatphys-020911-125101

Kranov, Y. A., Abuzir, A., Prakash, T., McIlroy, D. N., and Yeh, W. J. (2006). Barium Hexaferrite Thick Films Made by Liquid Phase Epitaxy Reflow Method. *IEEE Trans. Magn.* 42 (10), 3338–3340. doi:10.1109/TMAG.2006.879629

Kreisel, J., Pignard, S., Vincent, H., Sénateur, J. P., and Lucazeau, G. (1998). Raman Study of BaFe12O19 Thin Films. *Appl. Phys. Lett.* 73, 1194–1196. doi:10.1063/1.122124

Lavorato, G., and Winkler, E. (2016). Thickness Dependence of Exchange Coupling in Epitaxial. *Phys. Rev. B.* 94, 054405. doi:10.1103/PhysRevB.94.054405

Lisfi, A., and Williams, C. M. (2003). Magnetic Anisotropy and Domain Structure in Epitaxial CoFe2O4 Thin Films. *J. Appl. Phys.* 93 (10), 8143–8145. doi:10.1063/1.1541651

Liu, H., Avrutin, V., Xiao, B., Rowe, E., Liu, H. R., Özgür, Ü., et al. (2010). Epitaxial Relationship of MBE Grown Barium Hexaferrite (0001) Films on Sapphire (0001). *J. Cryst. Growth* 312 (5), 671–675. doi:10.1016/j.jcrysgro.2009.12.013

Malek, M. F., Mamat, M. H., Musa, M. Z., Soga, T., Rahman, S. A., Alrokayan, S. A. H., et al. (2015). Metamorphosis of Strain/stress on Optical Band gap Energy of ZAO Thin Films via Manipulation of thermal Annealing Process. *J. Lumin.* 160, 165–175. doi:10.1016/j.jlumin.2014.12.003

Masoudpanah, S. M., and Seyyed Ebrahimi, S. A. (2012). Synthesis and Characterization of Nanostructured Strontium Hexaferrite Thin Films by the Sol-Gel Method. *J. Magn. Magn. Mater.* 324 (14), 2239–2244. doi:10.1016/j.jmmm.2012.02.109

Masoudpanah, S. M., Seyyed Ebrahimi, S. A., and Ong, C. K. (2012). Effect of Oxygen Pressure on Microstructure and Magnetic Properties of Strontium Hexaferrite (SrFe12O19) Film Prepared by Pulsed Laser Deposition. *J. Magn. Magn. Mater.* 324 (7), 1440–1443. doi:10.1016/j.jmmm.2011.12.004

Meng, S., Yue, Z., and Li, L. (2012). In-plane C-axis Oriented Barium Hexaferrite Films Prepared by Magnetron Sputtering. *Mater. Lett.* 86, 92–95. doi:10.1016/j.matlet.2012.07.023

Meng, S., Yue, Z., Zhang, X., and Li, L. (2014). Quasi-epitaxial Barium Hexaferrite Thin Films Prepared by a Topotactic Reactive Diffusion Process. *Appl. Surf. Sci.* 290, 340–345. doi:10.1016/j.apsusc.2013.11.079

Meng, S., Yue, Z., and Li, L. (2014). Effect of Ethylene Glycol on the Orientation and Magnetic Properties of Barium Ferrite Thin Films Derived by Chemical Solution Deposition. *J. Magn. Magn. Mater.* 354, 290–294. doi:10.1016/j.jmmm.2013.11.016

Özgür, Ü., Alivov, Y., and Morkoç, H. (2009). Microwave Ferrites, Part 1: Fundamental Properties. J. Mater. Sci.: Mater. Electroni. 20 (9), 789–834. doi:10.1007/s10854-009-9923-2

Patel, R., Ikeda, Y., Onoda, H., Tainosho, T., Hisamatsu, Y., Sharmin, S., et al. (2018). Magnetic Properties of Epitaxial Barium Hexaferrite (0001) Thin Films Deposited by Radio Frequency Magnetron Sputtering. *IEEE Trans. Magn.* 54 (2), 1–4. doi:10.1109/TMAG.2017.2756687

Pullar, R. C. (2012). Hexagonal Ferrites: A Review of the Synthesis, Properties and Applications of Hexaferrite Ceramics. *Prog. Mater. Sci.* 57 (7), 1191–1334. Sep. 2012. doi:10.1016/J.PMATSCI.2012.04.001

Sun, K., Li, Q., Guo, H., Yang, Y., Yu, Z., Xu, Z., et al. (2016). Magnetic Property and Stress Study of Barium Hexaferrite Thin Films with Different Structures. *J. Alloys Compd.* 663, 645–650. doi:10.1016/j.jallcom.2015.12.193

Tang, R., Zhou, H., Zhao, R., Jian, J., Wang, H., Huang, J., et al. (2016). Dielectric Relaxation and Polaronic Conduction in Epitaxial BaFe12O19hexaferrite Thin Film. *J. Phys. D: Appl. Phys.* 49, 115305–115311. doi:10.1088/0022-3727/49/11/115305

Wang, Y. C., Ding, J., Yi, J. B., Liu, B. H., Yu, T., and Shen, Z. X. (2004). High-Coercivity Co-ferrite Thin Films on (100)-SiO2 Substrate. *Appl. Phys. Lett.* 84 (14), 2596–2598. Apr. 2004. doi:10.1063/1.1695438

Wei, G., Wei, L., Chen, Y., Yan, S., Mei, L., and Jiao, J. (2016). Self-assembled Epitaxial BaFe12O19 Nano-Island Film Grown on Al2O3 Substrate by Pulsed Laser Deposition. *Mater. Lett.* 181, 212–215. doi:10.1016/j.matlet.2016.06.006

Wei, X., Zheng, H., Chen, W., Wu, Q., Zheng, P., Zheng, L., et al. (2020). Crystal Structure, Morphology and Magnetic Properties of Hexagonal M-type Barium Ferrite Film Based on the Substrate Temperature. *Chem. Phys. Lett.* 752, 137541. doi:10.1016/j.cplett.2020.137541

Wu, Y., Yang, Q., Zhang, D., Zhang, Y., Rao, Y., Wen, Q., et al. (2020). The Submicron Garnet Film with Perpendicular Magnetic Anisotropy Prepared by Liquid Phase Epitaxy Method. *J. Magn. Magn. Mater.* 506, 166689. doi:10.1016/j.jmmm.2020.166689

Wu, M. (2012). M-type Barium Hexagonal Ferrite Films. *Adv. Magn. Mater.*, 33–60. doi:10.5772/39103

Xu, Z., Lan, Z., Sun, K., Yu, Z., Guo, R., Zhu, G., et al. (2013). Deposition of Perpendicular C -axis Oriented BaM Thin Films on (001) Al 2 O 3 Substrates by Introducing an Interfacial BaM Buffer Layer. *J. Magn. Magn. Mater.* 345, 72–76. doi:10.1016/j.jmmm.2013.06.018

Xu, Z. Y., Lan, Z. W., Sun, K., Yu, Z., Guo, R. D., Jiang, X. N., et al. (2013). Properties of Ba-Hexaferrite Thin Films with Different Layer Structures. *Amr* 774-776, 935–939. doi:10.4028/www.scientific.net/AMR.774-776.935

Yu, C., Sokolov, A. S., Kulik, P., and Harris, V. G. (2020). Stoichiometry, Phase, and Texture Evolution in PLD-Grown Hexagonal Barium Ferrite Films as a Function of Laser Process Parameters. *J. Alloys Compd.* 814, 152301. doi:10.1016/j.jallcom.2019.152301

Zhang, L., Su, X. D., Chen, Y., Li, Q. F., and Harris, V. G. (2010). Radio-frequency Magnetron Sputter-Deposited Barium Hexaferrite Films on Pt-Coated Si Substrates Suitable for Microwave Applications. *Scr. Mater.* 63 (5), 492–495. doi:10.1016/j.scriptamat.2010.05.013

Zhang, X., Yue, Z., Meng, S., and Yuan, L. (2014). Magnetic Properties of In-Plane Oriented Barium Hexaferrite Thin Films Prepared by Direct Current Magnetron Sputtering. *J. Appl. Phys.* 116, 243909–243924. doi:10.1063/1.4905028

Zhang, X., Meng, S., Song, D., Zhang, Y., Yue, Z., and Harris, V. G. (2017). Epitaxially Grown BaM Hexaferrite Films Having Uniaxial axis in the Film Plane for Self-Biased Devices. *Sci. Rep.* 7, 44193. doi:10.1038/srep44193

Zhang, X., Zhang, Y., Cao, S., Yue, Z., and Zhang, J. (2019). BaFe12O19 Films Prepared on Al2O3 (0 0 0 1) by Direct Current Magnetron Sputtering. *Mater. Lett.* 248, 24–27. doi:10.1016/j.matlet.2019.03.139

Zheng, H., Han, M., Zheng, L., Deng, J., Zheng, P., Wu, Q., et al. (2016). Magnetic Properties of Hexagonal Barium Ferrite Films on Pt/MgO(111) Substrates Annealed at Different Temperatures. *J. Magn. Magn. Mater.* 413 (111), 25–29. doi:10.1016/j.jmmm.2016.04.010

Zi, Z. F., Sun, Y. P., Zhu, X. B., Yang, Z. R., Dai, J. M., and Song, W. H. (2008). Structural and Magnetic Properties of SrFe12O19 Hexaferrite Synthesized by a Modified Chemical Co-precipitation Method. *J. Magn Magn. Mater.* 320 (21), 2746–2751. doi:10.1016/j.jmmm.2008.06.009

Conflict of Interest: The authors declare that the research was conducted in the absence of any commercial or financial relationships that could be construed as a potential conflict of interest.

Publisher's Note: All claims expressed in this article are solely those of the authors and do not necessarily represent those of their affiliated organizations, or those of the publisher, the editors and the reviewers. Any product that may be evaluated in this article, or claim that may be made by its manufacturer, is not guaranteed or endorsed by the publisher.